The EMBO Journal Vol. 20 No. 11 pp. 2611–2618, 2001

A structural pathway for activation of the kinesin motor ATPase

Mikyung Yun[1], Xiaohua Zhang[2], Cheon-Gil Park[1], Hee-Won Park[1,3,4] and Sharyn A.Endow[2,4]

[1]Department of Structural Biology, St Jude Children's Research Hospital, Memphis, TN 38105, [2]Department of Microbiology, Duke University Medical Center, Durham, NC 27710 and [3]Department of Biochemistry, University of Tennessee, Memphis, TN 38163, USA

[4]Corresponding authors
e-mail: hee-won.park@stjude.org or endow@duke.edu

Molecular motors move along actin or microtubules by rapidly hydrolyzing ATP and undergoing changes in filament-binding affinity with steps of the nucleotide hydrolysis cycle. It is generally accepted that motor binding to its filament greatly increases the rate of ATP hydrolysis, but the structural changes in the motor associated with ATPase activation are not known. To identify the conformational changes underlying motor movement on its filament, we solved the crystal structures of three kinesin mutants that decouple nucleotide and microtubule binding by the motor, and block microtubule-activated, but not basal, ATPase activity. Conformational changes in the structures include a disordered loop and helices in the switch I region and a visible switch II loop, which is disordered in wild-type structures. Switch I moved closer to the bound nucleotide in two mutant structures, perturbing water-mediated interactions with the Mg^{2+}. This could weaken Mg^{2+} binding and accelerate ADP release to activate the motor ATPase. The structural changes we observe define a signaling pathway within the motor for ATPase activation that is likely to be essential for motor movement on microtubules.

Keywords: ATPase activation/decoupling mutants/kinesin microtubule motors/structural changes

Introduction

Molecular motor proteins use the energy from ATP hydrolysis to move along cytoskeletal filaments, either actin or microtubules, producing work that can be used to contract muscles (Cooke, 1986), transport organelles and vesicles (Hirokawa, 1998; Brown, 1999), assemble spindles and move chromosomes (Endow, 1999) or drive cytokinesis (Goldberg *et al*., 1998). The mechanism by which motor proteins generate force and move on actin or microtubules is not yet understood. The ATPase activity of the motor is believed to increase greatly upon binding of the motor to its filament, enabling the motor to move along the filament, but the conformational changes associated with activation of the motor ATPase, and therefore required for motor movement, are not known.

Molecular motors undergo transitions between several distinct conformations that correspond to different nucleotide states as they hydrolyze ATP (reviewed in Cooke, 1986), e.g. a Mg·ATP prehydrolysis state, a Mg·ADP-P_i transition state and a Mg·ADP + P_i post-hydrolysis state. Workers anticipate that these nucleotide states and transitions between them will be detectable by spectroscopic or other analytical methods, or observed in crystal structures. Binding to actin or microtubules is expected to further change motor structure by causing structural changes in the filament-binding interface that are transmitted to the nucleotide-binding cleft, resulting in the greatly elevated ATPase activity that is observed when actin or microtubules are added to motors in ATPase reactions. For myosin, the structural changes associated with ATPase activation by actin are predicted to accelerate dissociation of ADP or P_i, the rate-limiting step in ATP hydrolysis (Lymn and Taylor, 1971), whereas for the kinesin motors, the structural changes induced by binding to microtubules should enable the motor to overcome the rate-limiting step, under non-saturating microtubule concentrations, of ADP release (Hackney, 1988).

Three different conformations of myosin have been observed in proteins crystallized with no nucleotide, a transition state analog or Mg·ADP (Rayment *et al*., 1993; Fisher *et al*., 1995; Dominguez *et al*., 1998; Houdusse *et al*., 1999). The models, interpreted to represent the motor in different states of the ATP hydrolysis cycle, have allowed workers to identify structural elements that undergo conformational changes during nucleotide hydrolysis (Fisher *et al*., 1995; Houdusse *et al*., 1999). In addition to a dramatic rotation of the lever arm, the 'switch I' and 'switch II' regions, which are structurally analogous to G protein elements that change in conformation upon nucleotide hydrolysis and exchange (Sablin *et al*., 1996), undergo movements that change the structure of the active site. The crystal structures of the kinesin motors have been less informative than those of myosin because, to date, they all contain Mg·ADP, despite attempts to crystallize the motors with different nucleotides or nucleotide analogs to obtain motors in different states. Comparisons of the available models have revealed only small differences (Sack *et al*., 1999), which are too small to classify the structures as distinct conformations. The kinesin crystal structures have therefore yielded little information thus far about the elements of the motor that move or change in conformation during nucleotide hydrolysis.

Identifying the conformational changes that convert the motor into a filament-activated state will be critical to understanding the mechanism of motility of the myosins and kinesins. Although the elevated ATPase produced by adding actin or microtubules to ATPase assays has been well documented, the mechanism by which the

enhancement of nucleotide hydrolysis occurs is not known. Recently, the relationship between the basal and microtubule-activated ATPase of the kinesin motors has been elucidated with the report of a mutant that separates the two activities by decoupling nucleotide and microtubule binding by the motor, preventing activation of the motor ATPase by microtubules (Song and Endow, 1998). The decoupling mutant binds tightly to both ADP and microtubules, unlike wild-type kinesin proteins, which bind weakly to microtubules in the presence of ADP, indicating that communication between the nucleotide- and microtubule-binding regions of the motor is disrupted. The change of a single amino acid residue in the mutant blocks activation of its ATPase by microtubules but does not block its basal ATPase activity, demonstrating that the basal and microtubule-activated ATPase activities of the motor can be separated from one another. Separation of the basal and microtubule-stimulated ATPase of the motor could occur by preventing structural changes that are required for ATPase activation and occur when the motor binds to microtubules.

Here we report the crystal structures of three kinesin mutants that block the microtubule-stimulated ATPase of the motor by decoupling nucleotide and microtubule binding by the motor, but do not block the basal ATPase activity of the motor. We interpret the decoupling mutants as destabilizing the ADP conformation and/or stabilizing conformations required to convert the motor into the microtubule-activated state. The structures show the first major changes in conformation of the kinesin motors to be observed in crystal structures. The structural changes that we observe identify elements of the motor that undergo movements during activation by microtubules and transmit the changes between the nucleotide- and microtubule-binding regions of the motor. The structural elements affected by the mutants define a signaling pathway for activation of the kinesin motor ATPase by microtubules.

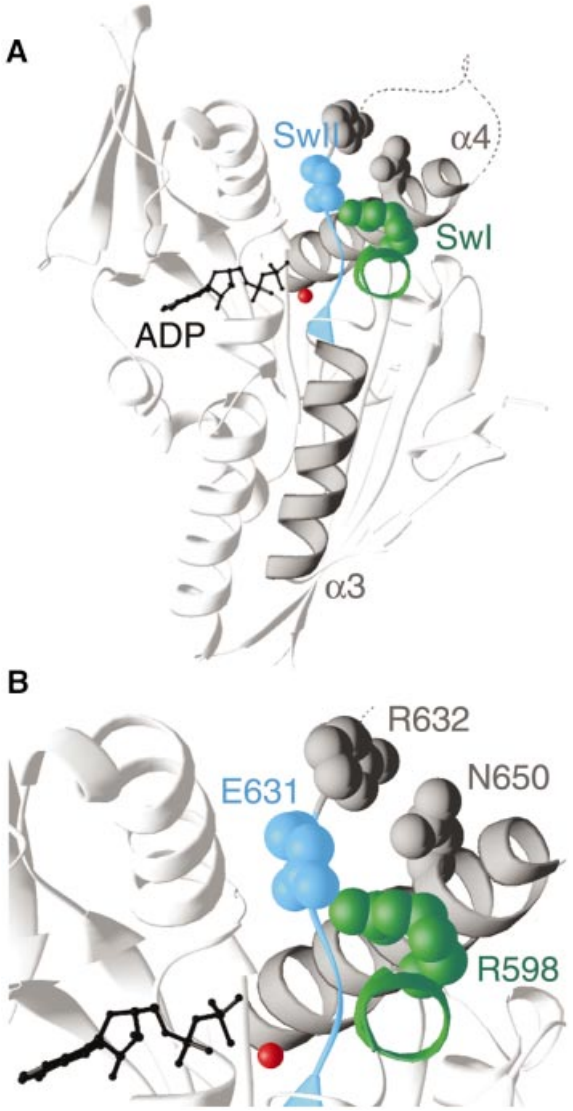

Fig. 1. Wild-type Kar3 and mutated residues. (**A**) The conserved switch I (SwI, green) and switch II (SwII, cyan) residues are indicated in Kar3+N11 together with helices α3 and α4 (gray). The switch II loop between R632 and the end of helix α4 (dotted line) is disordered and is not present in the model. Residues mutated in the Kar3 N650K uncoupling mutant (gray), Kar3 SwII R632A mutant (gray) and Kar3 salt-bridge mutants (R598A, green; E631A, cyan) are shown space-filled and enlarged in (B). (**B**) N650 of the Kar3 N650K uncoupling mutant interacts with R632 of SwII in wild-type Kar3. The salt bridge forms between R598 of SwI and E631 of SwII in wild-type Kar3. ADP (black) and Mg^{2+} (red) are shown as ball-and-stick models. Figure produced using RIBBONS (Carson, 1997).

Results

Mutants that block the microtubule-stimulated ATPase activity of the motor

The three mutants analyzed in this study were selected or designed to affect the microtubule-activated ATPase of the motor. The residues that were mutated are shown in the model of wild-type Kar3 (Figure 1). One of the mutations, Kar3 N650K, was found in a previous study to disrupt interactions between the microtubule- and nucleotide-binding regions of the motor (Song and Endow, 1998), as described above. The Kar3 N650K mutation completely blocks the microtubule-stimulated ATPase of the motor and prevents motility in gliding assays. The other two mutations, Kar3 R598A and Kar3 E631A, were designed to prevent formation of a salt bridge between the conserved switch I (SSRSH) and switch II (DLAGSE) regions of the motor, which has been observed in some, but not all kinesin crystal structures (Sack *et al*., 1999). Mutation of the corresponding salt-bridge residues in myosin inhibits or blocks ATPase activation by actin (Onishi *et al*., 1998; Furch *et al*., 1999).

The kinesin motors show a low basal ATPase activity, which is greatly stimulated by binding of the motor to microtubules, the cytoskeletal filaments along which the motors move. The ATP hydrolytic activity of wild-type Kar3 increases with increasing microtubule concentration (Figure 2A). As noted above, the Kar3 N650K decoupling mutant shows basal ATPase activity but, strikingly, shows no microtubule-stimulated ATPase activity in steady-state assays and methyl-anthraniloyl-ADP (mant-ADP) release was not accelerated by microtubules, in contrast to wild-type Kar3 (Song and Endow, 1998). When we analyzed the salt-bridge mutants, Kar3 R598A and Kar3 E631A, we found that neither mutant showed microtubule-activated ATPase activity in steady-state assays (Figure 2A),

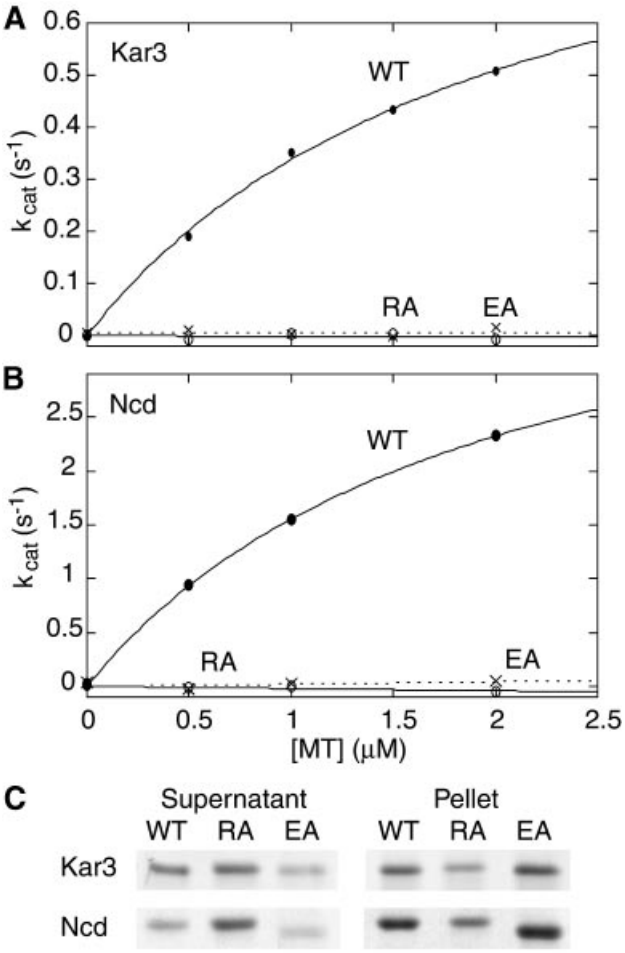

Fig. 2. ATPase activity and microtubule binding by salt-bridge mutants. Wild-type and mutant (**A**) Kar3 and (**B**) Ncd steady-state ATPase activity in the presence of microtubules; 1 μM motor protein + 0–2 μM microtubules. Wild type (WT; filled circles, —), RA (open circles, —), EA (×, - - -). (**C**) Microtubule binding by wild-type and mutant Kar3 and Ncd proteins. Coomassie Blue-stained motor protein in the supernatant (unbound) and pellet (microtubule-bound); 1 μM motor protein + 2 μM microtubules, no added nucleotide.

although both mutants showed basal ATPase activity similar to that of wild-type Kar3 (not shown).

The kinesin motors bind weakly to microtubules in the presence of Mg·ADP and tightly in the absence of nucleotide (Crevel *et al*., 1996), changing in binding affinity for microtubules during the ATP hydrolysis cycle. Unlike wild-type Kar3, the Kar3 N650K mutant binds tightly to microtubules even in the presence of Mg·ADP; the N650K mutation thus decouples nucleotide and microtubule binding by the motor (Song and Endow, 1998). The Kar3 R598A and Kar3 E631A mutants showed opposite effects to one another: Kar3 R598A bound weakly to microtubules in the presence of ADP or absence of nucleotide, whereas Kar3 E631A bound tightly. Under strong binding conditions (no added nucleotide), the dissociation constant (K_d) of Kar3 R598A from microtubules was higher than wild type (Kar3 R598A, K_d = 1.82 ± 0.66 μM; wild type, K_d = 0.37 ± 0.10 μM), and under weak binding conditions (+Mg·ADP) the K_d of Kar3 E631A was lower than wild type (Kar3 E631A, K_d = 0.27 ± 0.15 μM; wild type, K_d = 1.10 ± 0.49 μM). Relative binding by wild-type Kar3, Kar3 R598A and Kar3 E631A without added nucleotide is shown in Figure 2C.

Mutations were also made in the kinesin motor protein Ncd. Wild-type Ncd shows enhanced ATPase activity with increasing microtubule concentrations, but Ncd RA and Ncd EA showed no microtubule-activated ATPase activity (Figure 2B), like Kar3 R598A and Kar3 E631A. In microtubule pelleting assays, Ncd RA bound weakly to microtubules compared with wild type, whereas Ncd EA bound tightly (Figure 2C), paralleling the effects of Kar3 R598A and Kar3 E631A. These results demonstrate that the effects of mutating the salt-bridge residues are not specific to Kar3, as was also shown for the Kar3 N650K decoupling mutation (Song and Endow, 1998). This implies that a common pathway for ATPase activation by microtubules exists in the kinesin motors, coupled to changes in motor binding affinity for microtubules.

A high-resolution wild-type Kar3 motor domain structure

Wild-type Kar3+N11 contains 11 more amino acids at its N-terminus than Kar3 of the structure reported previously (Gulick *et al*., 1998) and behaves like a monomer in solution (Song and Endow, 1996). The structure of Kar3+N11 bound to Mg·ADP was determined to 1.5 Å resolution (Figure 1; Table I). Superposition of Kar3+N11 on the previous model showed an overall similarity (r.m.s. deviation of 0.7 Å). An unexpected finding was a conformational difference that caused helix α3 to be offset by 14° in the two structures, despite their identical crystallization conditions and space groups. A difference in helix α3 was observed previously in comparisons between kinesin and Ncd (Sablin *et al*., 1996; Sack *et al*., 1999) or Kar3 (Sack *et al*., 1999). Helix α3 thus appears to be inherently flexible, bending or moving at its C-terminus (Sack *et al*., 1999). Kar3+N11 also differed from the previous structure in the length of helix α4, which was three residues (approximately one turn) shorter, indicating that helix α4, together with the adjacent loop L11, which was disordered in both Kar3+N11 and the previous Kar3 structure, undergoes movement and can change in conformation.

Structure of the Kar3 N650K decoupling mutant

The structure of the Kar3 N650K decoupling mutant was determined to 1.7 Å resolution (Table I) and was found to be almost identical to wild type (r.m.s. deviation of 0.2 Å). The only difference was at the site of mutation in helix α4, where the side chains of N650 and R632 interact in wild-type Kar3, but the change of N650K in the mutant eliminated this interaction. R632 is present in the switch II loop, L11, adjacent to E631, which forms the salt bridge with R598 (Figure 1B). Disruption of the N650–R632 interaction could decouple microtubule and nucleotide binding, and block activation of the motor ATPase by disrupting transmission of the microtubule-binding signal to the active site. To test this idea, we mutated R632 to A and assayed the mutant motor for ATPase activity. The Kar3 SwII R632A mutant showed microtubule-stimulated ATPase activity that was reduced ~4-fold at 1 μM motor + 2 μM microtubules, compared with wild-type Kar3. The reduced activity provides evidence that the interaction of

Table I. X-ray diffraction data collection and refinement statistics

Motor protein	WT Kar3+N11	Kar3 N650K	Kar3 R598A	Kar3 E631A
Space group	$P2_1$	$P2_1$	$P2_1$	$P4_3$
Cell dimensions				
a (Å)	43.6	43.6	43.9	62.9
b (Å)	78.8	78.0	77.4	–
c (Å)	47.2	47.3	47.7	153.6
β (°)	105.0	105.1	105.9	–
Data collection				
resolution (Å)	20.0–1.5	20.0–1.7	20.0–1.3	20.0–2.5
measured reflections	793 427	309 408	929 216	265 649
unique reflections	47 889	31 822	70 750	20 874
completeness (%, > –3σ)[a]	97.3 (94.9)	93.5 (89.5)	94.0 (87.8)	96.0 (66.9)
R_{sym} (%)[b]	7.4	7.0	4.6	8.5
average $I/\sigma(I)$	16.2	17.5	41.7	18.8
Refinement				
R_{work}[c]	0.213	0.217	0.218	0.230
R_{free} (%)[c]	0.243	0.266	0.242	0.276
number of reflections [$F > 2\sigma$ (F)]	41 892	27 632	67 836	18 420
number of protein atoms	2 393	2 444	2 470	4 746
number of non-protein atoms	317	237	424	191
r.m.s.d.[d] bond length (Å)	0.006	0.006	0.006	0.009
r.m.s.d.[d] bond angles (°)	1.20	1.19	1.22	1.42
average B factors (Å^2, main chain/side chain)	19.6/22.3	22.3/24.6	15.2/17.8	42.3/44.8

[a]Last shell values are in parentheses. The last shell includes the resolution between 1.53 and 1.50 Å in Kar3+N11, 1.73 and 1.7 Å in Kar3 N650K, 1.32 and 1.3 Å in Kar3 R598A, and 2.59 and 2.5 Å in Kar3 E631A.
[b]$R_{sym} = \Sigma_{hkl}[\Sigma_i |I_{hkl,i} - \langle I_{hkl}\rangle|]/\Sigma_{hkl,i}\langle I_{hkl}\rangle$, where $I_{hkl,i}$ is the intensity of an individual measurement of the reflection with Miller indices h, k and l, and $\langle I_{hkl}\rangle$ is the mean intensity of that reflection.
[c]$R_{work} = \Sigma||F_{obs}| - |F_{calc}||/\Sigma|F_{obs}|$, where $|F_{obs}|$ and $|F_{calc}|$ are observed and calculated structure factor amplitudes, respectively. R_{free} is equivalent to R_{work} except that 10% of the total reflections were set aside to test the progress of refinement.
[d]R.m.s. deviation from ideal geometry.

N650 with R632 is involved in transmitting the microtubule-binding signal to the active site. But the failure of the mutant to completely block microtubule-stimulated ATPase activity indicates that an alternative pathway must exist to transmit the signal from N650 when this pathway is disrupted.

Structures of the salt-bridge mutants

The structure of the switch I salt-bridge mutant, Kar3 R598A, was determined to 1.3 Å resolution. The structure was similar to wild-type Kar3 but showed two major differences (Figure 3). First, loop L9 in the switch I region and the C-terminus of the adjacent helix α3, which interact with Mg^{2+}, were completely disordered. The N-terminus of the switch I helix α3a, which follows loop L9, was partially disordered. R598A was displaced toward loop L9 and helix α3 by 0.3 Å in Kar3 R598A compared with Kar3+N11, destabilizing loop L9, helix α3 and helix α3a. Secondly, loop L11, disordered in wild-type Kar3 structures, was visible. Three water molecules occupied the region of the missing side chain of R598. The carboxyl group of E645 of helix α4 moved by 1.3 Å to interact with E631 via the water molecules, stabilizing the N-terminus of helix α4 and loop L11. Mutation of R598A in Kar3 R598A thus destabilized the conformation surrounding switch I and stabilized the switch II loop–helix.

Crystals of the switch II mutant, Kar3 E631A, contained two identical molecules in an asymmetric unit. The Kar3 E631A structure, which was determined to 2.5 Å resolution, showed disordered switch I and switch II loops, L9 and L11. The N-terminus of the switch I helix α3a was disordered, whereas helix α3 was ordered (Figure 4). Unlike Kar3 R598A, R598 in Kar3 E631A maintained interaction with the switch II loop L11 by forming a new hydrogen bond to the carbonyl oxygen of G629. This suggests that complete disruption of interactions between the switch I and switch II loops is required to destabilize both loop L9 and the C-terminus of helix α3, as in Kar3 R598A. Loop L8 of Kar3 E631A was displaced by 2.3 Å compared with Kar3+N11 (Figure 4). Because loop L8 is implicated in microtubule binding (Woehlke *et al*., 1997; Alonso *et al*., 1998; Hirose *et al*., 1999; Kikkawa *et al*., 2000), it is possible that this structural change contributes to the tighter binding to microtubules by Kar3 E631A compared with wild type.

Discussion

The salt bridge between switch I and switch II

Previous crystal structures of the kinesin motors are complexed with Mg·ADP and have been interpreted to represent the ADP state of the motor. Slight differences exist between the structures (Sack *et al*., 1999), indicating that the structures could represent different intermediates in the ADP state. One of these differences is the presence or absence of a salt bridge between two highly conserved residues: the switch I R (SSRSH) and switch II E (DLAGSE). The salt bridge is present in four of the previous seven crystal structures of the kinesin motors, but it is absent in three of the structures: monomeric KHC (Kull *et al*., 1996) and Ncd (Sablin *et al*., 1996), and dimeric Ncd (Kozielski *et al*., 1999). Instead of the R–E salt bridge, the monomeric KHC and Ncd structures show movement of the R residue away from the E. The dimeric

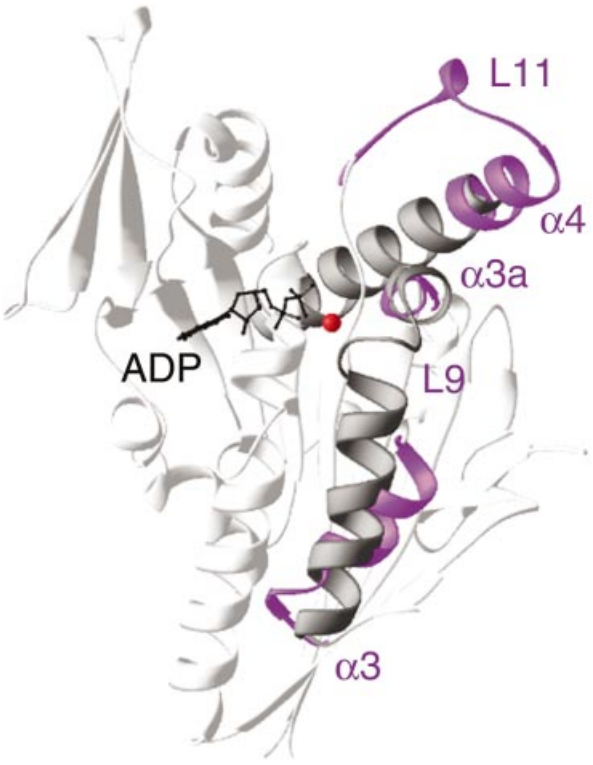

Fig. 3. Structural changes in Kar3 R598A. Kar3 R598A (purple) differs from wild-type Kar3+N11 (gray) in helices α4, α3a and α3, and loops L11 and L9. These structural elements define a signaling pathway that extends from helix α4 and loop L11 of switch II at the putative motor-microtubule binding interface (Woehlke *et al*., 1997; Alonso *et al*., 1998; Hirose *et al*., 1999; Kikkawa *et al*., 2000) to helix α3a and loop L9 of switch I, and helix α3, adjacent to the bound ADP (black) and Mg^{2+} (red). The disordered loop L9, N-terminus of helix α3a and C-terminus of helix α3 cause switch I to move towards the bound nucleotide and disrupt interactions with Mg^{2+}, which probably destabilizes the Mg^{2+} and accelerates release of ADP. Figure made with RIBBONS (Carson, 1997).

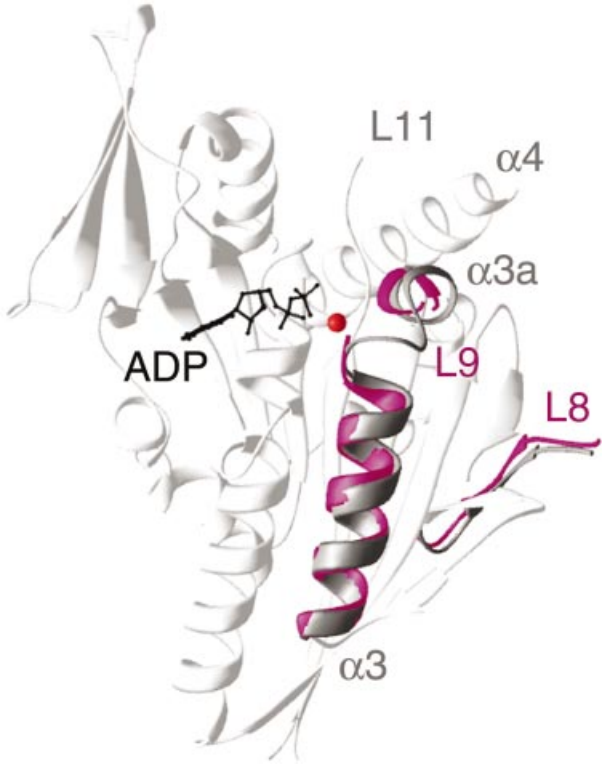

Fig. 4. Structural changes in Kar3 E631A. Kar3 E631A (magenta) differs from wild-type Kar3+N11 (gray) in loops L9 and L8. Loop L11 is disordered in both wild type and Kar3 E631A, and is not shown in the model. The disordered switch I loop L9 causes switch I to move towards the bound nucleotide. ADP, black; Mg^{2+}, red. Image prepared using RIBBONS (Carson, 1997).

Ncd structure of Kozielski *et al*. (1999) contains two dimers in the asymmetric unit, each with the salt-bridge residues in the two heads in close proximity to one another, but with missing ionic bonds between the residues. Interestingly, one of the heads of dimeric KHC (Kozielski *et al*., 1997) contains a salt bridge, but the other does not.

The salt bridge is also observed in the myosins, where it again forms between highly conserved switch I R (SSRFG) and switch II E (DIXGFE) residues. In the myosins, the salt bridge is thought to stabilize the 'closed' conformation of the motor (Geeves and Holmes, 1999) in which the nucleotide cleft is closed around the bound nucleotide. In the closed conformation, the γ-phosphate of the bound nucleotide is hydrogen bonded to the invariant switch II G, and coordinated by the Mg^{2+} ion and the invariant P loop K, e.g. myosin S1 complexed with ADP·vanadate (Smith and Rayment, 1996). Mutation of the salt-bridge residues severely reduces the basal ATPase of the motor and inhibits or blocks activation of myosin by actin (Onishi *et al*., 1998; Furch *et al*., 1999). These effects can be attributed to stabilization by the salt bridge between switch I and switch II of the closed conformation, which is thought to be essential for nucleotide hydrolysis (Geeves and Holmes, 1999).

The nucleotide binding cleft in the kinesins is exposed to the surface of the protein rather than enclosed between two domains of the protein, as in myosin, and it is therefore not certain that a state exists in the kinesin motors that is analogous to the closed conformation of myosin. Despite this, our results show that mutation of the corresponding salt-bridge residues in two kinesin motors, Kar3 and Ncd, blocks activation of the motor by microtubules. This indicates that an intact salt bridge between the switch I and switch II regions of the motor is required for activation of the kinesin motors by microtubules, as it is for activation of myosin by actin. We further show that mutation of the salt-bridge residues in Kar3 causes conformational changes that trap the motor in a weak (Kar3 R598A) or strong (Kar3 E631A) microtubule-binding state. Results from proteolytic mapping experiments (Alonso *et al*., 1998), alanine-scanning mutagenesis (Woehlke *et al*., 1997) and cryo-electron microscopy (Hirose *et al*., 1999; Kikkawa *et al*., 2000) implicate helix α4 and loops L11 and L8 in interfacing with the microtubule. Stabilization of loop L11 and the N-terminus of helix α4 in Kar3 R598A could prevent tight binding of the motor to the microtubule and cause the weak binding to microtubules observed for the Kar3 R598A mutant. The strong binding to microtubules by Kar3 E631A may be due to the displacement of loop L8 compared with wild type. Remarkably, these changes in motor binding affinity for microtubules are caused by mutations of single residues, which may not themselves

Table II. Distance from the bound nucleotide and Mg^{2+} to switch I residues

Motor protein	P_α to	S596	S597	R598
WT Kar3+N11		10.45	9.33	12.99
Kar3 R598A		10.58	9.16	12.84
Kar3 E631A		9.66	8.93	12.58
	Mg^{2+} to	S596	S597	R598
WT Kar3+N11		6.23	5.64	9.08
Kar3 R598A		6.23	5.32	8.86
Kar3 E631A		5.52	4.95	8.50

Distances are in angstroms and were measured using the program O (Jones *et al.*, 1991). Kar3 N650K is almost identical to wild-type Kar3+N11 and is therefore not shown.

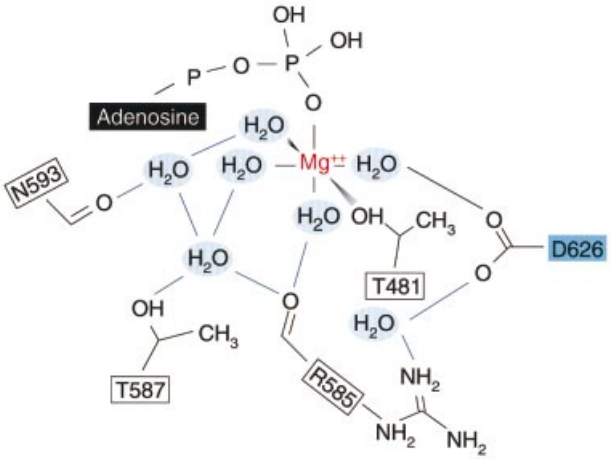

Fig. 5. Coordination of the Mg^{2+} ion in wild-type Kar3. The bound Mg^{2+} of wild-type Kar3 has a tetragonal bipyramidal or octahedral coordination due to the P_β oxygen, the hydroxyl group of T481 and four water molecules that also interact with D626 of switch II (cyan), R585 and T587 of loop L9, and N593 of helix α3a. R585 is hydrogen bonded by a water molecule to the D626 side chain that interacts with the Mg^{2+}.

interact directly with tubulin. The Kar3 N650K mutant also shows tighter binding to microtubules than wild-type Kar3, like Kar3 E631A, but this can be attributed at least in part to the nature of the mutation: a change of N650 to a positively charged K in helix α4, an element that is thought to interface directly with tubulin, would be predicted to cause the motor to bind more tightly to microtubules.

Structural changes in the mutants

All three of the Kar3 mutant structures we report are complexed with Mg·ADP, like the previous kinesin crystal structures, but Kar3 R598A and Kar3 E631A show changes that differ from the ADP conformations reported previously. A major change in Kar3 R598A, not observed previously in other kinesin crystal structures, is the partial melting of helix α3. Furthermore, loop L9 and the N-terminus of helix α3a are disordered in both Kar3 R598A and Kar3 E631A, causing switch I to be displaced towards the bound nucleotide and Mg^{2+} ion (Table II), which perturbs interactions with the Mg^{2+}. In wild-type Kar3, the Mg^{2+} is coordinated in a tetragonal bipyramidal or octahedral geometry by a β-phosphate oxygen, the hydroxyl group of T481, and four water molecules that also interact with D626 of switch II, R585 and T587 of loop L9, and N593 of helix α3a (Figure 5). A water-mediated hydrogen bond between R585 and D626 stabilizes the side chain of D626 that interacts with the Mg^{2+}. The water-mediated interactions of the Mg^{2+} with R585, T587 and N593 are disrupted in Kar3 R598A and Kar3 E631A because loop L9 and the region of helix α3a that contains N593 are disordered. Disruption of these interactions probably causes the Mg^{2+} to be more weakly bound in the mutants than in wild-type Kar3. Movement of R585 is likely to have a dual effect on the binding of the Mg^{2+} by (i) disrupting its own water-mediated interactions with the Mg^{2+} and (ii) destabilizing D626, which also indirectly coordinates the Mg^{2+} via a water molecule. Release of the Mg^{2+} is predicted to accelerate release of ADP, the rate-limiting step in kinesin nucleotide hydrolysis under non-saturating microtubule concentrations (Hackney, 1988), activating the motor ATPase.

In addition to these structural changes in the switch I region, Kar3 R598A shows changes in the switch II region of the motor compared with wild-type Kar3. The changes include stabilization of loop L11 and the N-terminus of helix α4, the switch II loop–helix. In Kar3 R598A, helix α4 begins at G640 instead of R644, as in wild-type Kar3, extending the length of helix α4 by one turn. This is not substantially different from the length of helix α4 in the previous wild-type Kar3 model, however, where helix α4 begins at R641 (Gulick *et al.*, 1998). The Kar3 R598A and wild-type Kar3 models demonstrate that helix α4 can undergo changes in length of as much as a turn by melting of residues at its N-terminus. Helix α4 therefore appears to be intrinsically unstable. The switch II loop L11 is visible in Kar3 R598A, differing from its disordered state in wild-type Kar3 structures and in Kar3 E631. Stabilization of loop L11 may be the basis of the weak binding by Kar3 R598A to microtubules compared with wild type or Kar3 E631A, as noted above.

The disordering or melting of helix α3 (Kar3 R598A) and helix α3a (Kar3 R598A, Kar3 E631A), and the changes in the length of helix α4 (Kar3 R598A cf. wild-type Kar3) resemble the melting of the SH1 helix in myosin. In myosin the disordered SH1 helix causes a marked change in angle of the lever arm, which may play an essential role in the contractile cycle (Houdusse *et al.*, 1999). Helix melting thus occurs in at least three helices of Kar3, as well as in myosin, and appears to represent a common mechanism used by the kinesin and myosin motors to move domains to enable motor function.

The structures we observe for Kar3 R598A and Kar3 E631A differ from previous structures reported for the kinesin motors. The dramatic structural changes in the proteins compared with previous models cause us to believe that they are not merely due to inherent flexibility of the switch I and switch II regions. It is possible that the structures correspond to kinetic intermediates of the ADP state detected by others using spectrophotometric methods (Xing *et al.*, 2000), or they may represent previously unobserved ADP→ATP transition states. Binding of the motor to microtubules is likely to cause even more extensive changes that involve the same structural elements as those we have identified here to undergo movements. The changes in Kar3 R598A and Kar3 E631A that

probably underlie activation of the ATPase involve movement of switch I toward the bound nucleotide, resulting in weaker binding of the Mg^{2+} and accelerated ADP release. This differs from the movements that occur in myosin during conversion of the motor from the closed to the open form. The closed state, thought to be required for nucleotide hydrolysis, undergoes transition to the open form, proposed to be associated with actin binding and P_i release, by movement of the switch II region out of the active site (Fisher *et al*., 1995; Geeves and Holmes, 1999).

A pathway for activation of the motor by microtubules

The Kar3 R598A and Kar3 E631A salt-bridge mutants and the Kar3 N650K mutant (Song and Endow, 1998) show basal ATPase activity in steady-state assays similar to that of wild-type Kar3. The kinetics of mant-ADP release by the Kar3 N650K mutant in the absence of microtubules was also found to be close to that of wild-type Kar3 (Song and Endow, 1998). The Kar3 R598A and Kar3 E631A salt-bridge mutants were not analyzed using transient methods in the present study. Further analysis of the salt-bridge mutants, as well as the Kar3 N650K uncoupling mutant, may reveal changes in the basal ATPase (Rice *et al*., 1999) that are detectable only using single-turnover or transient methods. The findings relevant to the work presented here are that the salt-bridge and uncoupling mutants can hydrolyze nucleotide and bind to microtubules, but they fail to show enhanced ATPase activity in the presence of microtubules. This indicates that nucleotide and microtubule binding by the motor are decoupled in all three mutants. The mutants decouple nucleotide and microtubule binding by disrupting transmission to the nucleotide-binding cleft of changes that occur in the motor upon binding to microtubules. The mutant effect of blocking activation of the motor by microtubules and the structural elements the mutants affect define a pathway within the motor for activation by microtubules that extends from helix α4 at the putative motor–microtubule binding interface to the nucleotide-binding cleft (Figures 1 and 3). We propose that, upon binding to microtubules, the signal for activation of the Kar3 ATPase is transmitted from N650 of helix α4 to R632 of L11, then to the E–R salt bridge and from the salt bridge to the active site (Figure 1B).

This pathway is supported by evidence that helix α4 of the kinesin motors interfaces with the microtubule (Woehlke *et al*., 1997; Alonso *et al*., 1998; Hirose *et al*., 1999; Kikkawa *et al*., 2000) and by the complete block in ATPase activation of the mutants. Mutation of Kar3 R632 to A reduced, but did not abolish, microtubule-enhanced ATPase activity, indicating that an alternative pathway of activation must exist in Kar3. N650 of Kar3 helix α4 is invariant in the known kinesin proteins, but Kar3 R632 is replaced by K in KHC and by S in Ncd. Structures of both KHC (Sack *et al*., 1997) and Ncd (Kozielski *et al*., 1999) show the N of helix α4 hydrogen bonded to the salt bridge/switch I R, which is also invariant in the kinesin motors, indicating that the microtubule-binding signal is transmitted directly to the salt bridge via the conserved switch I R in KHC and Ncd. This could serve as an alternative pathway in Kar3, and would consist of transmission of the microtubule-binding signal from N650 of helix α4 to switch I R598 and the E–R salt bridge, and from the salt bridge to the active site.

The E–R salt bridge in the kinesin motors thus provides a direct means of communication between switch I and switch II to enable the signal for microtubule binding to be transmitted to the active site. The effect of the Kar3 R598A and Kar3 E631A mutants in completely blocking the microtubule-activated ATPase of the motors provides evidence that direct interactions between switch I and switch II are required for activation of the kinesin motors by microtubules. The pathway of structural changes that we observe in the Kar3 motor identifies changes in the switch I and switch II regions that the motor undergoes during activation of its ATPase by microtubules. These changes are likely to be essential for motor movement along microtubules and will therefore be critical to understanding the structural basis of kinesin motor-based transport in the cell.

Materials and methods

Protein expression, purification and biochemical assays

Plasmids encoding the RA and EA mutants were made by PCR (Ho *et al*., 1989) and confirmed by DNA sequencing. Kar3 mutant proteins corresponded to residues 383–729 and Ncd proteins to residues 333–700 of the full-length protein. Protein purification and biochemical tests were as described (Song and Endow, 1996, 1998). Kar3 E631A was expressed with or without His_6 at its N-terminus. Tests of the His_6 protein gave K_d values in microtubule-binding assays that overlapped those of the non-tagged protein and His_6-Kar3 E631A showed basal ATPase activity but no microtubule-stimulated ATPase activity in nucleotide hydrolysis assays. Basal ATPase activity was assayed using Mg·[γ-^{32}P]ATP and activated charcoal binding of unhydrolyzed nucleotide (Chandra *et al*., 1993). Microtubule-binding assays for K_d determination were performed in 10 mM HEPES pH 7.2, 50 mM NaCl, 1 mM EGTA and 1 mM $MgCl_2$; the assays in Figure 2C were in 50 mM Tris–acetate pH 7.5, 50 mM NaCl, 1 mM EGTA, 1 mM $MgCl_2$ and 100 μg/ml bovine serum albumin (Hackney and Stock, 2000). Two or more ATPase or microtubule-binding experiments with wild-type Kar3 or Ncd controls were performed for each mutant (Kar3 R598A, Kar3 E631A, Kar3 SwII R632A, Ncd RA, Ncd EA) protein.

Crystallization and structure determination

Crystals were grown at 18°C (Kar3+N11, Kar3 N650K) or 4°C (Kar3 R598A, His_6-Kar3 E631A) in hanging drops consisting of 2 μl of protein (15 mg/ml) + 2 μl of well solution containing 20–26% PEG2000ME and 0.2 M NaCl as precipitants, and 50 mM HEPES buffer pH 7.0–8.0 (Gulick *et al*., 1998). Diffraction data were collected at Brookhaven National Synchrotron Light Source beamline X4A using a Brandeis Q4 CCD detector operating at 100°K, and processed using HKL (Otwinowski and Minor, 1997). The structure of native Kar3+N11 was determined by refining the previous model of the Kar3 motor domain (Gulick *et al*., 1998) using the Kar3+N11 data at 1.5 Å resolution. From the resulting electron density map, we were able to build the side chains of residues that were built as alanines in the previous model. The structures of Kar3 N650K and Kar3 R598A were determined by refining the final model of Kar3+N11 using diffraction data at 1.7 and 1.3 Å resolution, respectively. X-PLOR (Brünger, 1992) was used for crystallographic refinement and the model was built in the programs O (Jones *et al*., 1991) and XtalView (McRee, 1998). The Kar3 R598A mutant contained Mg·ADP bound to the active site even in crystals grown in the presence of AMP·PNP. In addition to the Mg·ADP bound to the P loop, the model for Kar3 R598A shows a second ADP bound to a cleft between helix α1 and strand β8. This is probably an artifact due to a spurious ionic interaction, since the Mg^{2+} was missing and the site was not fully occupied. The structure of Kar3 E631A was determined by molecular replacement using the refined Kar3+N11 as a search model at 2.5 Å resolution. The cross-rotation and translation functions and Patterson correlation refinement were calculated using X-PLOR. The two best solutions for the rotation search corresponded to two molecules of the Kar3 motor domain in the asymmetric unit. After the relative translation between the two molecules was determined, the model containing both molecules was subjected to

rigid body refinement, resulting in an *R* factor of 38.0%. Several iterations of refinement and model building improved the structure (see Table I). Non-crystallographic symmetry restraints were applied throughout the refinement.

Accession numbers

The atomic coordinates (accession codes 1F9T, 1F9U, 1F9V and 1F9W) have been deposited in the Protein Data Bank.

Acknowledgements

The Kar3 R598A and Kar3 E631A salt-bridge mutants were designed by A.Gulick and the *kar3* mutant plasmids were made by H.Song. We thank C.Ogata and his staff at beamline X4A, supported by the Howard Hughes Medical Institute, and C.R.Ross for help with diffraction data collection. This work was supported by NIH grants to St Jude Children's Research Hospital Cancer Center and S.A.E., an American Heart Association grant to H.-W.P., an American Lebanese Syrian Associated Charities grant to H.-W.P. and a Human Frontier Science Program grant to S.A.E.

References

Alonso,M.C., van Damme,J., Vandekerckhove,J. and Cross,R.A. (1998) Proteolytic mapping of kinesin/ncd-microtubule interface: nucleotide-dependent conformational changes in the loops L8 and L12. *EMBO J.*, **17**, 945–951.

Brown,S.S. (1999) Cooperation between microtubule- and actin-based motor proteins. *Annu. Rev. Cell Dev. Biol.*, **15**, 63–80.

Brünger,A.T. (1992) *X-PLOR, A System for X-ray Crystallography and NMR*. Yale University Press, New Haven, CT.

Carson,M. (1997) Ribbons. *Methods Enzymol.*, **277**, 493–505.

Chandra,R., Salmon,E.D., Erickson,H.P., Lockhart,A. and Endow,S.A. (1993) Structural and functional domains of the *Drosophila* ncd microtubule motor protein. *J. Biol. Chem.*, **268**, 9005–9013.

Cooke,R. (1986) The mechanism of muscle contraction. *CRC Crit. Rev. Biochem.*, **21**, 53–118.

Crevel,I.M.-T.C., Lockhart,A. and Cross,R.A. (1996) Weak and strong states of kinesin and ncd. *J. Mol. Biol.*, **257**, 66–76.

Dominguez,R., Freyzon,Y., Trybus,K.M. and Cohen,C. (1998) Crystal structure of a vertebrate smooth muscle myosin motor domain and its complex with the essential light chain: visualization of the pre-power stroke state. *Cell*, **94**, 559–571.

Endow,S.A. (1999) Microtubule motors in spindle and chromosome motility. *Eur. J. Biochem.*, **262**, 12–18.

Fisher,A.J., Smith,C.A., Thoden,J.B., Smith,R., Sutoh,K., Holden,H.M. and Rayment,I. (1995) X-ray structures of the myosin motor domain of *Dictyostelium discoideum* complexed with MgADP·BeF_x and MgADP·AlF_4^-. *Biochemistry*, **34**, 8960–8972.

Furch,M., Fujita-Becker,S., Geeves,M.A., Holmes,K.C. and Manstein,D.J. (1999) Role of the salt-bridge between switch-1 and switch-2 of *Dictyostelium* myosin. *J. Mol. Biol.*, **290**, 797–809.

Geeves,M.A. and Holmes,K.C. (1999) Structural mechanism of muscle contraction. *Annu. Rev. Biochem.*, **68**, 687–728.

Goldberg,M.L., Gunsalus,K.C., Karess,R.E. and Chang,F. (1998) Cytokinesis. In Endow,S.A. and Glover,D.M. (eds), *Dynamics of Cell Division*. Oxford University Press, Oxford, UK, pp. 270–316.

Gulick,A.M., Song,H., Endow,S.A. and Rayment,I. (1998) X-ray crystal structure of the yeast Kar3 motor domain complexed with MgADP to 2.3 Å resolution. *Biochemistry*, **37**, 1769–1776.

Hackney,D.D. (1988) Kinesin ATPase: rate-limiting ADP release. *Proc. Natl Acad. Sci. USA*, **85**, 6314–6318.

Hackney,D.D. and Stock,M.F. (2000) Kinesin's IAK tail domain inhibits initial microtubule-stimulated ADP release. *Nature Cell Biol.*, **2**, 257–260.

Hirokawa,N. (1998) Kinesin and dynein superfamily proteins and the mechanism of organelle transport. *Science*, **279**, 519–526.

Hirose,K., Löwe,J., Alonso,M., Cross,R.A. and Amos,L.A. (1999) Congruent docking of dimeric kinesin and ncd into three-dimensional electron cryomicroscopy maps of microtubule-motor ADP complexes. *Mol. Biol. Cell*, **10**, 2063–2074.

Ho,S.N., Hunt,H.D., Horton,R.M., Pullen,J.K. and Pease,L.R. (1989) Site-directed mutagenesis by overlap extension using the polymerase chain reaction. *Gene*, **77**, 51–59.

Houdusse,A., Kalabokis,V.N., Himmel,D., Szent-Györgyi,A.G. and Cohen,C. (1999) Atomic structure of scallop myosin subfragment S1 complexed with MgADP: a novel conformation of the myosin head. *Cell*, **97**, 459–470.

Jones,T.A., Zou,J.Y., Cowan,S.W. and Kjeldgaard,M. (1991) O. *Acta Crystallogr. A*, **47**, 110–119.

Kikkawa,M., Okada,Y. and Hirokawa,N. (2000) 15 Å resolution model of the monomeric kinesin motor, KIF1A. *Cell*, **100**, 241–252.

Kozielski,F., Sack,S., Marx,A., Thormählen,M., Schönbrunn,E., Biou,V., Thompson,A., Mandelkow,E.-M. and Mandelkow,E. (1997) The crystal structure of dimeric kinesin and implications for microtubule-dependent motility. *Cell*, **91**, 985–994.

Kozielski,F., De Bonis,S., Burmeister,W.P., Cohen-Addad,C. and Wade,R.H. (1999) The crystal structure of the minus-end-directed microtubule motor protein ncd reveals variable dimer conformations. *Structure*, **7**, 1407–1416.

Kull,F.J., Sablin,E.P., Lau,R., Fletterick,R.J. and Vale,R.D. (1996) Crystal structure of the kinesin motor domain reveals a structural similarity to myosin. *Nature*, **380**, 550–555.

Lymn,R.W. and Taylor,W.E. (1971) Mechanism of adenosine triphosphate hydrolysis by actomyosin. *Biochemistry*, **10**, 4617–4624.

McRee,D.E. (1998) *XtalView v.3.2.1*. The Scripps Research Institute, La Jolla, CA.

Onishi,H., Kojima,S., Katoh,K., Fujiwara,K., Martinez,H.M. and Morales,M.F. (1998) Functional transitions in myosin: formation of a critical salt-bridge and transmission of effect to the sensitive tryptophan. *Proc. Natl Acad. Sci. USA*, **95**, 6653–6658.

Otwinowski,Z. and Minor,W. (1997) Processing of X-ray diffraction data collected in oscillation mode. *Methods Enzymol.*, **276**, 307–326.

Rayment,I., Rypniewski,W.R., Schmidt-Base,K., Smith,R., Tomchick,D.R., Benning,M.M., Winkelmann,D.A., Wesenberg,G. and Holden,H.M. (1993) Three-dimensional structure of myosin subfragment-1: a molecular motor. *Science*, **261**, 50–58.

Rice,S. *et al*. (1999) A structural change in the kinesin motor protein that drives motility. *Nature*, **402**, 778–784.

Sablin,E.P., Kull,F.J., Cooke,R., Vale,R.D. and Fletterick,R.J. (1996) Crystal structure of the motor domain of the kinesin-related motor ncd. *Nature*, **380**, 555–559.

Sack,S., Müller,J., Marx,A., Thormählen,N., Mandelkow,E.-M., Brady,S.T. and Mandelkow,E. (1997) X-ray structure of motor and neck domains from rat brain kinesin. *Biochemistry*, **36**, 16155–16165.

Sack,S., Kull,F.J. and Mandelkow,E. (1999) Motor proteins of the kinesin family. Structure, variations and nucleotide binding sites. *Eur. J. Biochem.*, **262**, 1–11.

Smith,C.A. and Rayment,I. (1996) X-ray structure of the magnesium(II)·ADP·vanadate complex of the *Dictyostelium discoideum* myosin motor domain to 1.9 Å resolution. *Biochemistry*, **35**, 5404–5417.

Song,H. and Endow,S.A. (1996) Binding sites on microtubules of kinesin motors of the same or opposite polarity. *Biochemistry*, **35**, 11203–11209.

Song,H. and Endow,S.A. (1998) Decoupling of nucleotide- and microtubule-binding in a kinesin mutant. *Nature*, **396**, 587–590.

Woehlke,G., Ruby,A.K., Hart,C.L., Ly,B., Hom-Booher,N. and Vale,R.D. (1997) Microtubule interaction site of the kinesin motor. *Cell*, **90**, 207–216.

Xing,J., Wriggers,W., Jefferson,G.M., Stein,R., Cheung,H.C. and Rosenfeld,S.S. (2000) Kinesin has three nucleotide-dependent conformations. Implications for strain-dependent release. *J. Biol. Chem.*, **275**, 35413–35423.

Received January 29, 2001; revised and accepted March 29, 2001